Investigation of the Azraq Basin in the Eastern Desert of Jordan using Integrated Geoelectrical Techniques

P. Yogeshwar[1], B. Tezkan[1], A. Haroon[1]
[1]Institute of Geophysics and Meteorology, Cologne, Germany
Email: yogeshwar@geo.uni-koeln.de, CRC-806: Our Way to Europe, www.sfb806.de

The Eastern Mediterranean has been the passageway for human migration between Africa, the Middle East, the Balkans and Europe. The Azraq basin in the eastern desert of Jordan has been a major spot for human settlements since the middle Pleistocene. The former lake in the basin center has developed to a hyper-saline alluvial mudflat, the Qa' Al Azraq. In the mudflat thick sequences of alluvial sediments are deposited. Such sediment successions are promising archives used for reconstructing the paleoclimate.
We utilized the Transient Electromagnetic (TEM), the Direct Current Resistivity (DCR) and the Radiomagnetotelluric (RMT) methods to identify suitable borehole locations in the area for the paleoclimatical reconstruction. Two transects were investigated from the edge of the basin to the basin center.
The data sets of the three methods are interpreted by 1D Marquardt and Occam inversion. Furthermore, the DCR data is interpreted by a 2D smoothness constraint inversion. Previously uncertain geological boundaries are determined by the geoelectrical models along both transects.

1 Introduction

The Collaborative Research Centre 806 (CRC 806) *Our Way to Europe* concerns the history of mankind. It is designed to capture the complex nature of dispersal of modern man from Africa to Western Eurasia, and particularly to Europe. The CRC 806 concentrates on the time span between the dispersal of modern man from Africa (190,000 B.P.) and the permanent establishment in Central Europe (40,000 B.P.). The CRC 806 investigates archaeological sites, terrestrial and aquatic archives in the source region of modern man, along trajectories of dispersal and in sink areas (Fig. 1). It is a multidisciplinary project established at the Universities of Cologne, Bonn and Aachen [SFB-806, 2012].

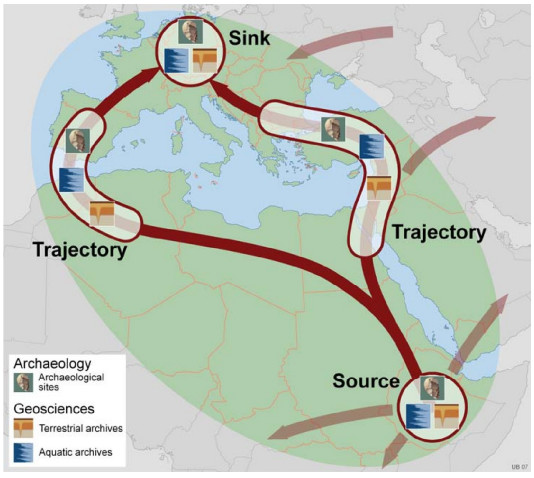

Figure 1: *Study areas of the CRC 806: the source region, trajectories and sink areas [SFB-806, 2012].*

The Eastern Mediterranean has been the passageway for human migration between Africa, the Middle East, the Balkans and Europe. In particular the Jordan rift valley served as a trajectory of dispersal of modern man [SFB-806, 2012].
The Azraq area is located 100 km east of Amman, in the eastern desert of Jordan (Fig. 2). The area around the former oasis Qa' Al Azraq has been a major spot for prehistoric settlements since the middle Pleistocene [Gerard et al., 1975; Copeland, 1988; Byrd, 1988]. The former shorelines of the Qa' Al Azraq mudflat are littered with stone artifacts, which were also found during the geophysical field survey.
Very promising archives for paleoclimatical reconstruction are sediment successions accumulated in dry clay lakes. Davies [2005] has analyzed a 31 m long core from the Qa' El Jafr basin in the south of Jordan and provided paleoclimate data for the Jordan Plateau. Ahmad [2010] interpreted the paleoclimate and paleoenvironment by dating bulk organic matter from the Azraq area. Abed et al. [2008] suggest the presence of a varying fresh to brackish water lake throughout the history, covering an area of roughly 13,000 km^2 around 330,000 B.P. The former lake in the center of the Azraq Basin has developed to a 10×10 km^2 big hyper-saline alluvial mudflat, the Qa' Al Azraq. During rainy season it is partly covered by water. In the basin center thick sequences of alluvial sediments, consisting mostly of clay intermixed with various evaporates, are deposited.
The Azraq area is of enormous economical importance to Jordan, due to its mineral deposits and groundwater resources. Approximately one third of the freshwater supply for Jordan's capital city Amman is provided from the Azraq Area [Ibrahim, 1996].
El-Kaysi and Talat [1996] and El-Waheidi et al. [1992] studied the condition of the shallow aquifer system and the interface of the fresh-brackish water zone utilizing Schlumberger vertical electric soundings.

In the present studies, previously uncertain depths of geological boundaries are determined and from that, suitable borehole locations for the paleoclimatical re-

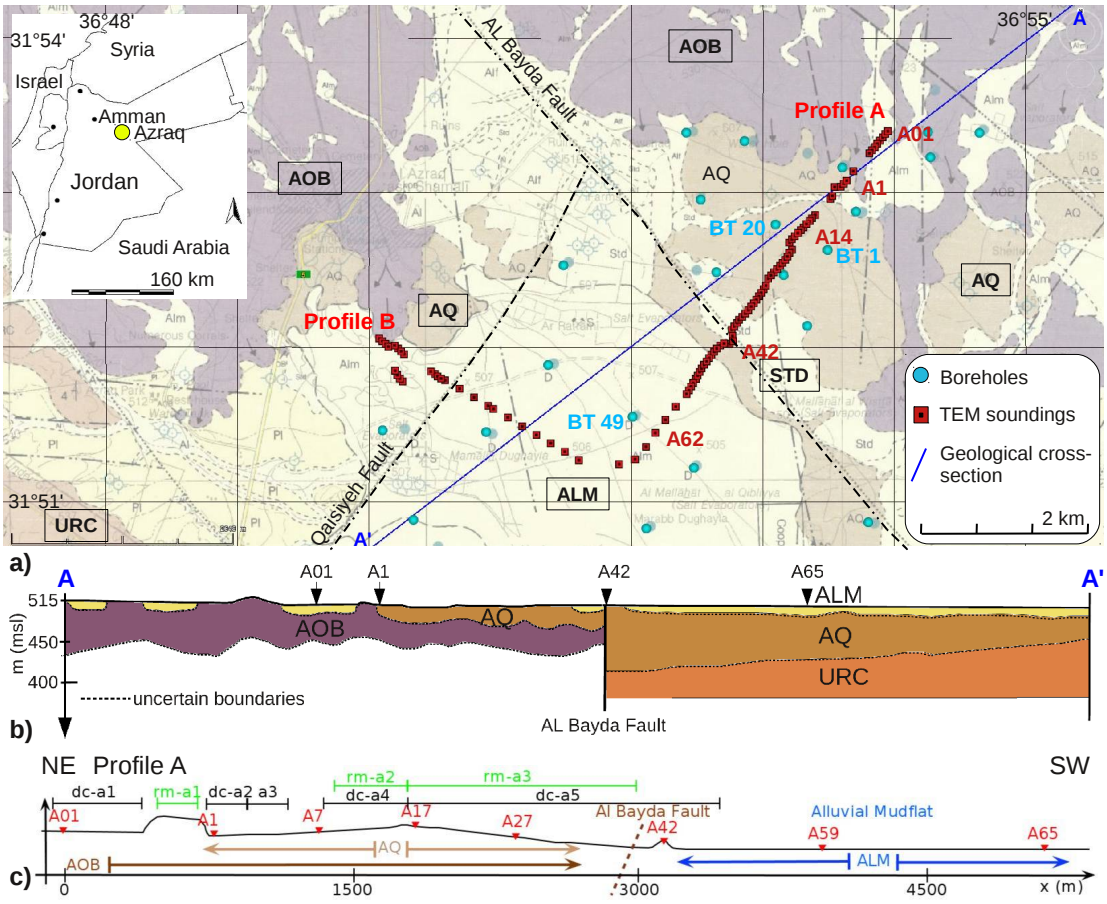

Figure 2: *(a) Geological map of the survey area. (b) Geological cross section for AA' (Modified after Ibrahim [1996]). The TEM stations are marked with red squares and labeled A01 to A65. (c) Schematic sketch of DCR and RMT profiles investigated on profile A. TEM stations are marked as red triangles, DCR profiles are marked black and RMT profiles green. AQ: Azraq Quaternary Formation, AOB: Abed Olivine Phyric Basalt, URC: Umm Rijam Chert Limestone Formation, ALM: Alluvial Mudflat.*

construction are identified. Two transects, 5 km and 3 km long, were investigated from the edge of the basin to the basin center, crossing three geological formations. We utilized the Transient Electromagnetic (TEM), the Direct Current Resistivity (DCR) and the Radiomagnetotelluric (RMT) methods.
The TEM data is interpreted by 1D Marquardt and Occam inversions and stitched together as a 2D section for the complete profile. For the time being, the RMT data is interpreted for selected stations in a similar manner as the TEM data. The DCR data is interpreted in 2D using a smoothness constraint inversion. The geoelectrical models are calibrated with lithological information available in the survey area.

2 Geology and hydro-geology of the study area

The geological features occurring in the Azraq area are briefly described in Ibrahim [1996].
The Azraq basin is a tectonic structural depression. It covers an area of 30×50 km^2, oriented from northwest to southeast, situated roughly 500 m above mean sea level. It is bounded by two major fault systems, the Fuluq fault in the north and the As Sirhan fault in the south.
The 10×10 km^2 Qa' Al Azraq in the basin center is bounded by faults from all sides. In the northeast the Al Bayda fault is present and in the northwest the Qaisiyeh fault (Fig. 2).
Four geological formations are described in the study area and were investigated during the geophysical field survey.

1. The Abed Olivine Phyric Basalt (AOB) stems from the earliest volcanism in the area. It is most abundant, highly fractured and forms irregular shaped boulders. It outcrops in the northern area.

2. The Umm Rijam Chert Limestone Formation (URC) outcrops in the northeast and southwest and forms the base of the mudflat.

3. The Azraq Quaternary Formation (AQ) consists of clay, intermixed with various evaporates and

fragments of gravel, limestone and basalt. The top surface is a present erosion and deposition surface, partly covered by alluvial sediments. At station A42 the AQ is covered by the Dasha Silt Dunes (STD).

4. The Alluvial Mudflat (ALM) in the basin center consists of soft, silty hyper saline clays intermixed with various evaporates. Beneath the ALM quaternary sediments of the AQ formation are present. The depth down to the URC formation is roughly 80 m [El-Kaysi and Talat, 1996].

These formations are displayed in the geological map (Fig. 2(a)). In the cross-section in Fig. 2(b), the depth of the geological boundaries are uncertain and therefore marked as dotted lines.

Three Aquifer systems were defined in the basin [Ibrahim, 1996]. The ground water occurrence in the upper aquifer system is complex, due to to the high lithological variability. The ground water level ranges between 250 m depth in the northern lava fields and less than 6 m in the Qa Al' Azraq. The main groundwater recharge is from the north.
Due to high evaporation the groundwater is hypersaline inside the alluvial mudflat with an electrical resistivity of around 2 Ωm.
The upper aquifer is extensively exploited for agricultural purpose and freshwater supply for Jordan's capital Amman. The extreme groundwater discharge has lead to a drastic decline of the ground water table.

3 Field measurement and data interpretation

Two transects were investigated from the edge of the mudflat to the center. Profile A is oriented from northeast to southwest and has a total length of 5130 m. Profile B is oriented from northwest to southeast and has a length of 3250 m.
The TEM measurements were carried out utilizing a NT-20 transmitter and a GDP32 receiver unit [Zonge, 2002]. A total of 102 stations were investigated (Profile A: 74 stations, Profile B: 28 stations). In general the station distance was 50 m between each consecutive station, depending on the availability of space and probable noise sources (e.g. 50 Hz powerlines) in the field. On the mudflat the station distance was increased to 200 m. The transmitter loop size was 50×50 m^2 and the receiver loop (single turn) was 10×10 m^2.
We measured in two modes: NanoTEM (NT) and ZeroTEM (ZT). The NanoTEM mode records 31 logarithmic equidistant values of the induced voltage in a time window from t =7.28E-07 to 1.91E-03 s. Setting the device to ZeroTEM mode allows to record from t =3.81E-05 to 2.43E-02 s.
Profile A was additionally investigated with DCR and RMT. The DCR measurements were performed using an ABEM SAS 4000 multi-electrode system [ABEM, 2010]. The length of the Wenner array was decided, depending upon the availability of space. Five DCR profiles (dc-a1 to dc-a5, (Tab. 1)) were investigated and are displayed in Fig. 2(c).

DCR profile	dc-a1	dc-a2	dc-a3	dc-a4	dc-a5
length (m)	400	200	150	600	1700
El. sep. (m)	2.5	2.5	2.5	5	5

Table 1: *DCR profiles investigated on the profile A.*

The RMT measurements were performed with the RMT-F device from the University of Cologne [RMT-F, 2005; Tezkan and Saraev, 2007; Tezkan, 2009]. Three RMT profiles were investigated on profile A (length: rm-a1= 150 m, rm-a2= 350 m, rm-a3=1320 m) with a distance of 10 m between consecutive stations (Fig. 2(c)). Usually seven distinct frequencies were available in the range from 10 kHz to 1 MHz in the E-polarization (TE-mode). The strike direction was assumed in southeast direction, i.e. aligned with the Al Bayda fault. Therefore, transmitters associated with the electric field directions perpendicular to the profile and parallel to the assumed strike direction were assumed as the E-polarization.

3.1 Data processing

Due to the self- inductance of the TEM transmitter loop, the current turn-off is not instant. The transmitter turn-off time (ramp time) depends on the current, the loop size and the subsurface resistivity distribution. For the configuration used during the field survey the ramp time was 3.5 μs in NanoTEM and 56 μs in ZeroTEM mode [Zonge, 2002].
The relation between a linear current turn-off function and the induced voltage was described by Fitterman and Anderson [1987]. We removed the effect of the linear ramp by applying a parameterized deconvolution of the measured signal and the current turn-off function. Afterwards both, the Nano- and ZeroTEM transients are stitched together to one long transient [Lange, 2003; Helwig et al., 2003; Hanstein, 1992]. Data points with standard deviations higher than $\Delta d = 3\%$ are removed.
The DCR and RMT data is edited visually for data outliers. In particular for DCR, data points with high standard deviations are removed from the apparent resistivity pseudosection. We assumed a percentage error of $\Delta d = 3$ % for the DCR and RMT data.
The processed TEM, DCR and RMT data for station A14 on profile A is presented in Fig. 3. The TEM data is transformed from induced voltages into late-time-apparent resistivities [Ward and Hohmann, 1988]. From the TEM and DCR data a resistor in the depth is indicated, which is not indicated by the RMT data, due to an insufficient depth of investigation for the lowest available frequency.

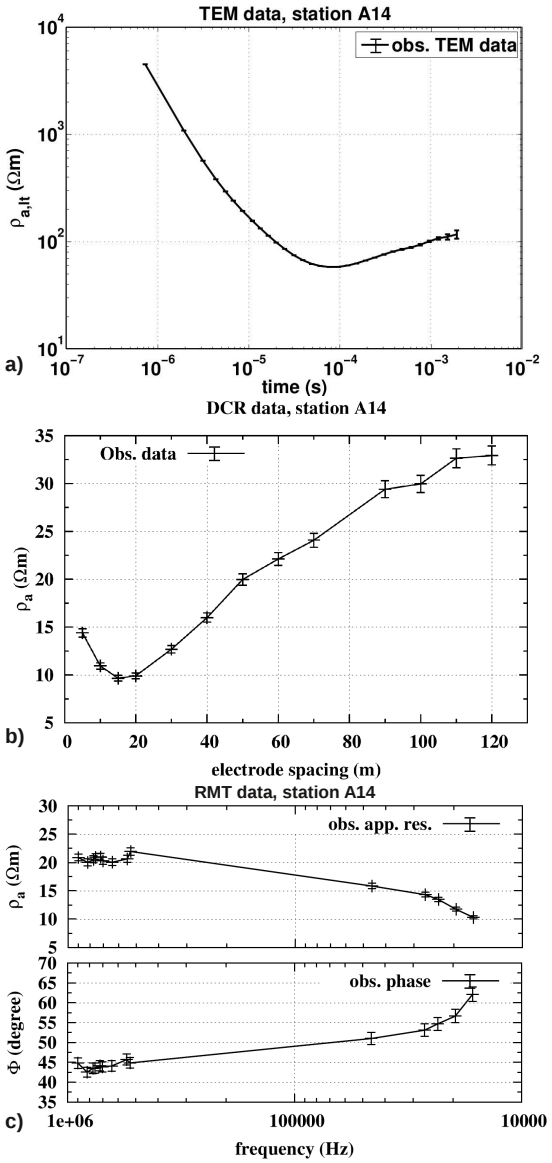

Figure 3: *(a) TEM, (b) DCR and (c) RMT data observed on profile A, station A14.*

3.2 1D interpretation of the data

The observed data is analyzed using a 1D inversion. We use the Occam scheme implemented for the first (Occ R1) and second order smoothness (Occ R2) constraint of the model [Constable et al., 1987]. The first and second order Occam inversion models generally differ in zones, where the model is not supported by the data. In order to obtain a layered earth model, Marquardt inversions are performed, too [Scholl, 2005; Menke, 1984]. For both, Occam and Marquardt inversion, a homogeneous halfspace model is used as an initial guess. The number of model layers for the Marquardt inversion is derived from the result of the particular Occam inversion model.
The obtained Marquardt best-fit and the corresponding equivalent models for station A14, investigated on the AQ formation, are displayed in Fig. 4(a),(b) and (c). The 1D results for station A62 on the mudflat is displayed in Fig. 4(f).
Besides calculating equivalent models, another possibility for the model resolution appraisal is to analyze the resulting matrices of a singular value decomposition of the generalized inverse during the Marquardt inversion [Scholl, 2005]. The importance of each model parameter is calculated according to Menke [1984]. The closer the value is to one, the better the model parameter is resolved.
The data fit is estimated according to the Root Mean Square (RMS)

$$RMS = \sqrt{\frac{1}{N}\sum_{i=1}^{N}\frac{(d_{i,obs}-d_{i,calc})^2}{(d_{i,obs})^2}} \qquad (1)$$

where $d_{i,obs}$ is the observed data, $d_{i,calc}$ the calculated data and N is the number of data points.
The depth of investigation (DOI) of the TEM method, is estimated according to Spies and Frischknecht [1991]:

$$\delta_{doi} = 0.5\left(\frac{IA\bar{\rho}}{\eta}\right) \qquad (2)$$

where I is the transmitted current, A the transmitter loop size and $\bar{\rho}$ is the mean resistivity of the overlying subsurface. We assume that the transients were always recorded until the noise level is reached, therefore η corresponds with the induced voltage value of the last recorded time point.
The obtained 1D models for station A14 (Fig. 4(a) to (c)) are matching well and validate each other. Especially the TEM and DCR models coincide. Further more the Marquardt and Occam models are well comparable.
According to the model parameter importances, the first layer of the TEM model (Fig. 4(c)) is not resolved separately. The third layer resistivity shows acceptable equivalence and is resolved with an importance of 0.38. The last layer resistivity and depth is resolved again well ($Imp > 0.8$).
The RMT model in Fig. 4(a) is reliable down to a depth of 15 m, due to the limited depth of investigation. Therefore, the last layer ist not significant. The latter is clear, due to the low importance values for the last layer, the huge equivalence and the differing of the two Occam models in a depth of 15 m.
The Marquardt and Occam models for station A62 are coinciding. Nevertheless, the resistivities of the second and fourth layer are not resolved, according to the Marquardt inversion models.

3.2.1 Correlation with borehole lithological data

Lithological borehole data was available from a bentonite drilling project in the Azraq area [Ibrahim, 1996; Ala'li, 1993]. The geoelectrical models are compared and calibrated with the lithological data. The locations of the boreholes used (BT-1 and BT-49) are

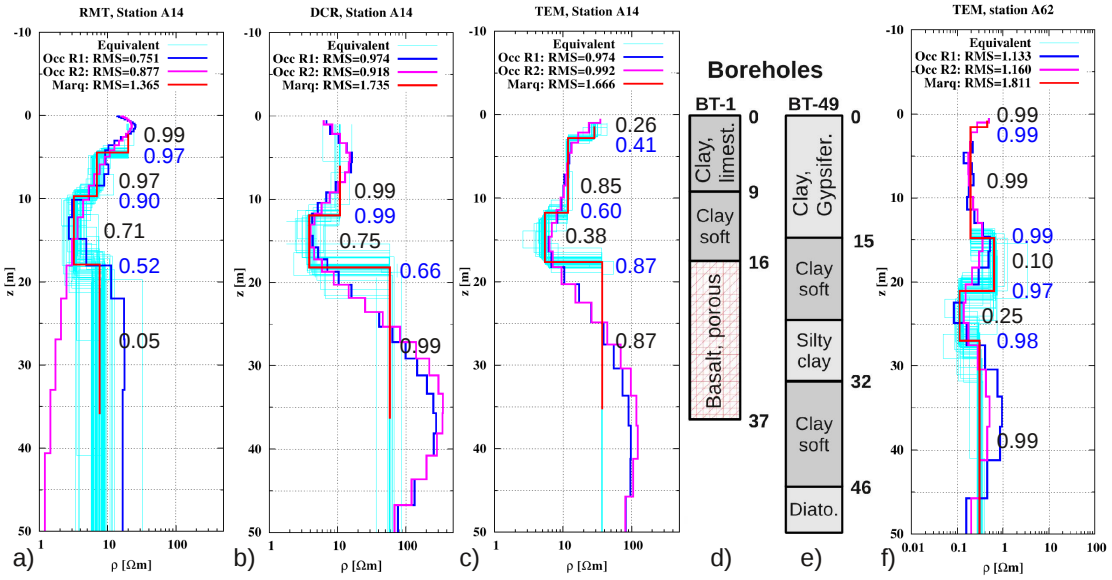

Figure 4: *1D inversion models of (a) TEM, (b) DCR and (c) RMT data for station A14 obtained on the AQ formation. Borehole lithological information for (d) BT-1 on the AQ formation and (e) BT-49 on the mudflat (Shown on the geological map (Fig. 2)). 1D inversion models of (f) the TEM data for station A62 on the mudflat. The importance for each layer resistivity and thickness is displayed in black and blue, respectively.*

displayed in Fig. 2.

According to the borehole data of BT-1 (Fig. 4(d)), the topmost 12 m of the model for station A14 consists of a clay layer intermixed with evaporates, pieces of limestone, chert, gravel and plant roots. The resistivity range is between 10 to 20 Ωm. Below, a soft clay layer is present with a resistivity of around 3 Ωm. In a depth of 16 m the basalt is clearly detected with a resistivity of around 40 to 100 Ωm. The basalt is highly porous and intermixed with gypsiferous material [Ibrahim, 1996].

The TEM resistivity model for station A62 on the alluvial mudflat is calibrated with lithological data from borehole BT-49 (Fig. 4(e)), which consists of layers of hyper-saline gypsiferous clay, soft clay, silty clay and diatomite. Both models, Marquardt and Occam, correlate quite well with the lithological data. However, the resistivity contrasts for the TEM models are small and the equivalent models indicate poorly resolved layers with resistivities ranging between 0.1 and 1 Ωm.

3.3 2D interpreted sections

We have calculated the TEM late-time apparent resistivity ($\rho_{a,lt}$) and the first order time derivative (Fig. 5(b) and (c), respectively). There are some data gaps along the profile, due to topography, streets and a powerline. Between $x = 750$ and 1000 m along the profile line a more conductive zone is visible at approximately $t = 10^{-4}$ s. Southwest of the Al Bayda fault, $\rho_{a,lt}$ decreases strongly to around 0.5 Ωm.

The first order time derivative of $\rho_{a,lt}$ visualizes a probable resistivity increase in the depth. Fig. 5(b) indicates a resistive structure in the depth between $x = 0$ and 3000 m, starting at approximately $t = 10^{-4}$ s. The increase of the $\rho_{a,lt}$-values obviously stems from the basalt layer. On the alluvial mudflat, northwest of station A42, only a slight increase of $\rho_{a,lt}$ is visible for very late times, indicating a resistor in the depth.

The calculated 1D TEM inversion models are stitched together as a 2D section for all 74 stations along profile A (Fig. 6(a) and (b)). We did not apply any constraints between neighbouring models or fix regions with a-priori information.

The 2D stitched section for the Marquardt 4 layer models and the Occam R2 models are displayed in Fig. 6(a) and (b), respectively. Both 2D sections are matching very well.

In a depth of 495 m amsl the basalt layer is present. It is slightly dipping downwards towards southwest and ends at the Al Bayda fault. The top of the basalt is precisely determined by the stitched TEM models. From $x = 700$ m to 3000 m a quite thin soft clay layer is present above the basalt, which is also described in the lithological information (Fig. 4). The top surface layer with a resistivity of 6 to 25 Ωm coincides with the clay layer, intermixed with pieces of chert, limestone and gravel. The quaternary sediments above the basalt stream belong to the AQ-formation.

Southwest of the Al Bayda fault the alluvial mudflat begins. It contains of hyper-saline clays. The resistivity varies between 0.1 and 1 Ωm. A slight layering is visible from the 2D stitched Occam models inside the ALM. Although the resistivity contrast is small it is continues in lateral direction. Apparently this layering coincides with the different type of clays described in the lithological information (Fig. 4). As supported by the time derivative of the first order late-time apparent resistivity, a slight increase of the

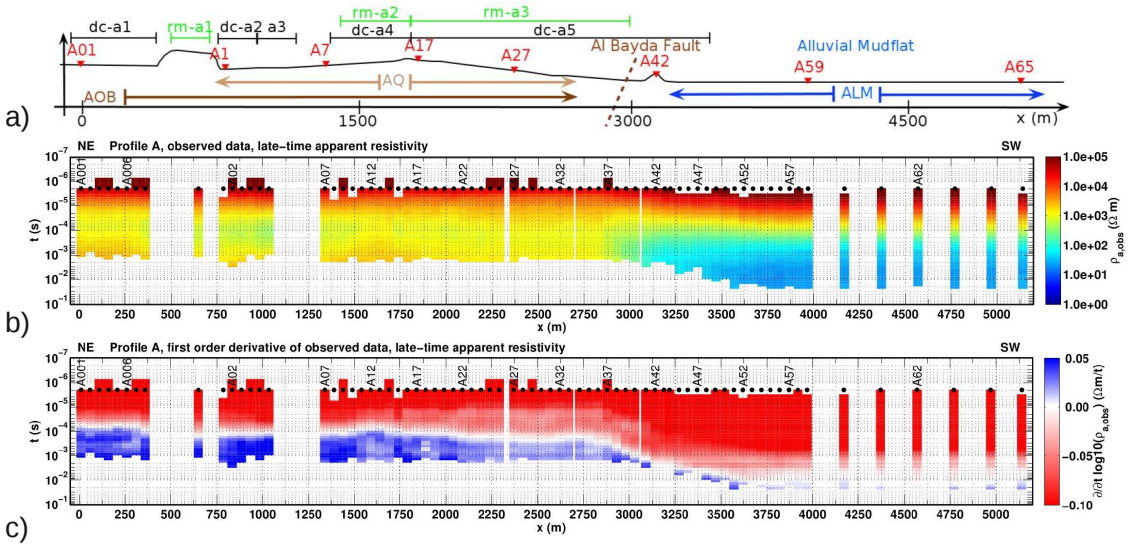

Figure 5: *(a) Schematic sketch of the investigated profiles along Profile A. 2D section of (b) TEM late-time apparent resistivity data and (c) first order time derivative of TEM late-time apparent resistivity data.*

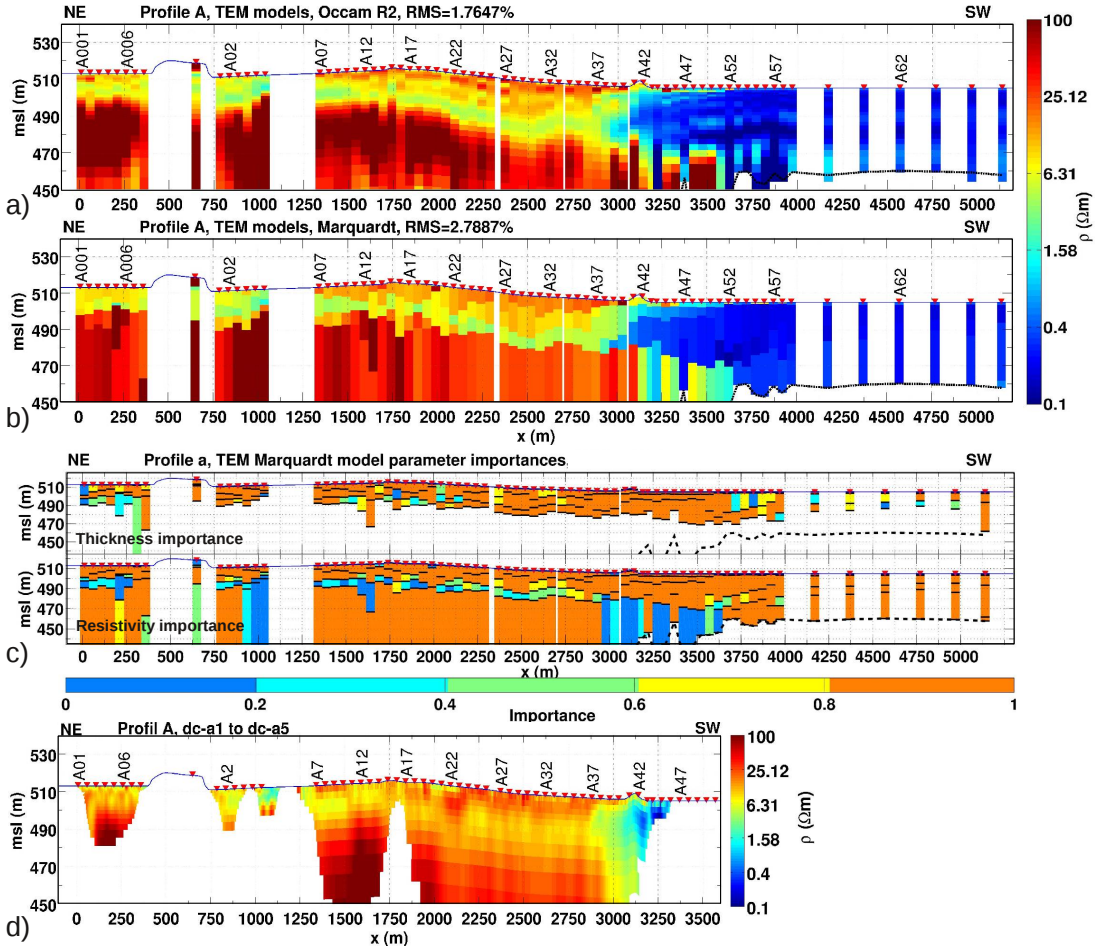

Figure 6: *1D inversion results stitched together as a 2D section for (a) the Marquardt models (b) the Occam R2 models. (c) 2D section of the importances of each layer thickness and resistivity for each station. (d) 2D DCR inversion models. The DOI is plotted as a dotted line in the TEM models inside the mudflat.*

model resistivity is visible in a depth of 480 m amsl. From the geological cross section, the deposited alluvial sediments inside the mudflat are followed by quaternary sediments of the AQ formation, which are also present northeast of the mudflat. Most likely the slight increase in resistivity in about 480 m amsl, is related to the top of the AQ formation. Deeper resistivity information is not available, due to a limited DOI of roughly 50 m on the mudflat (Fig. 6(a),(b)).
In the transition zone, close to the Al Bayda fault, the subsurface becomes highly two-dimensional and a 1D interpretation becomes inadequate. From both, the data and the models, it is not clear if the basalt stream continues after $x = 3000$ m towards southeast until $x = 3600$ m. Therefore we have calculated the importances for each layer resistivity and thickness (plotted as a 2D section in Fig. 6(c)). According to the latter, the top of the last layer is well resolved, whereas the resistivity is not resolved in the transition zone.
The data for all 74 stations is fitted with a glabal RMS of 1.76% for the Occam models and 2.79% for the Marquardt models.

The DCR data is inverted in 2D using a second order smoothness constraint inversion algorithm by Günther [2004]. The smoothness parameter is determined automatically in each inversion iteration by the L-curve criterion [Hansen and O'Leary, 1993]. We have masked the zones in the models which are not supported by the data.
The DCR profiles (dc-a1 to dc-a5) are plotted along profile A in Fig. 6(d). For the large Wenner arrays (dc-a1, dc-a4 and dc-a5) the basalt stream is well detected. The overlying clay layer is represented a bit more resistive than in the stitched TEM models (Fig. 6(b)). The transition zone is visible at around $x = 3000$ m along the profile line. Further southwest, DCR measurements were not possible due to technical problems. Therefore, the continuation of the basalt southwest of the Al Bayda fault is unclear from the DCR result.

4 Conclusions

Two long transects were investigated in the Azraq area from the edge of the Qa Al' Azraq to the center, utilizing three geophysical methods: TEM, DCR and RMT.
The TEM data is analyzed in detail. A 5 km long 2D subsurface resistivity section is derived from stitched Occam and Marquardt inversion models. The resulting models are appraised by equivalent modelling and inversion statistics (i.e. model parameter importances). The DCR data is interpreted in 2D and the obtained models validate the 2D stitched TEM section.
Three geological formations are investigated in the study area. Previously uncertain geological boundaries are determined by the geophysical results. Especially the depth down to the basalt stream is detected, which is a limitation for probable future drilling projects. A geological layering inside the alluvial mudflat could be identified, which also coincides with the lithological data. The transition zone between the basalt stream and the alluvial mudflat is resolved, although the subsurface is highly two-dimensional and the 1D interpretation becomes critical.
The Azraq area has a tremendous importance to Jordan, due to its mineral and water resources. This study provides additional geological information. Furthermore it is a basis for future drilling projects.

5 Acknowledgement

The project is funded by the DFG and hosted in the frame of the CRC-806 "Our Way to Europe", established at the Universities of Cologne, Bonn and Aachen. We gratefully thank the Natural Resources Authority, Jordan and especially Tahsin Talat for great support in the field work, the tough organization and the hospitality.

6 References

Abed, A. M., Yasin, S., Sadaqa, R., Al-Hawari, Z., 2008. The paleoclimate of the eastern desert of jordan during marine isotope stage 9. Quaternary Research 69, 458–468.

ABEM, 2010. Terrameter SAS 4000 / SAS 1000 Instruction Manual. ABEM Instrument AB, printed matter no. 93109 Edition.
URL http://www.abem.se/software.php

Ahmad, K. I., 2010. Organic chemistry of Al-Azraq basin, Jordan, an interpretation of paleoenvironment and paleoclimate using bulk organic matter. Ph.D. thesis, University of Missouri-Kansas City.

Ala'li, J., 1993. Exploration for Bentonite and other Minerals in Azraq Depression. Tech. rep., Natural Recources Authority, Geology Directorate, Economic Geology Division, Amman.

Byrd, B. F., 1988. Late Pleistocene settlement diversity in the Azraq basin. Paleorient 14/2, 257–264.

Constable, S. C., Parker, R. L., Constable, C. G., 1987. Occam's inversion: a practical algorithm for generating smooth models from EM sounding data. Geophysics 52, 289–300.

Copeland, L., 1988. Environment, chronology and lower-middle-paleolithic occupations of the Azraq basin, Jordan. Paleorient 14/2, 66–75.

Davies, C., 2005. Quaternary paleoenvironment and potential for human exploitation of the Jordan plateau interior. Geoarchaeology: An International Journal 20/4, 379–400.

El-Kaysi, K., Talat, T., 1996. Geoelectrical survey in the Azraq mudflat area. Tech. rep., Natural Resources Authority, Geophysics and Technical Service Department, Geophysics Division, Amman.

El-Waheidi, M., Merlanti, F., Pavan, M., 1992. Geoelectrical resistivity survey of the central part of Azraq basin (Jordan) for identifying saltwater/freshwater interface. Journal of Applied Geophysics 29, 125–133.

Fitterman, D., Anderson, W., 1987. Effect of Transmitter Turn-Off Time on Transient Soundings. Geoexploration 24, 131–146.

Gerard, A. N., Price, N. S., Copeland, L., 1975. A survey of prehistoric sited in the Azraq basin, eastern Jordan. Paleorient 3, 109–126.

Günther, T., 2004. Inversion Methods and Resolution Analysis for the 2D/3D Reconstruction of Resistivity Structures from DC Measurements. Ph.D. thesis, Technische Universität Bergakademie Freiberg.

Hansen, P. C., O'Leary, D. P., 1993. The use of the l-curve in the regularization of discrete ill-posed problems. SIAM Journal of Scientific Computing 14, 1487–1503.

Hanstein, T., 1992. Iterative und parametrisierte Dekonvolution für LOTEM Daten. In: Protokoll über das 14. Kolloquium Elektromagnetische Tiefenforschung. Dt. Geophys. Gesellschaft, p. 163–172.

Helwig, S. L., Lange, J., Hanstein, T., 2003. Kombination dekonvolvierter Messkurven zu einem langen Transienten. In: Protokoll über die 63. Jahrestagung der Deutschen Geophysikalischen Gesellschaft. Dt. Geophys. Gesellschaft.

Ibrahim, K., 1996. The Regional Geologoy of Al Azraq Area. Hashemite Kingdom of Jordan, Geological Mapping Division, Natural Resources Authority, Bulletin 36.

Lange, J., 2003. Joint Inversion von Central-Loop-TEM und Long-Offset-TEM Transienten am Beispiel von Messdaten aus Israel 2002. Master's thesis, Universität zu Köln, Institut für Geophysik und Meteorologie.

Menke, W., 1984. Geophysical data analysis: discrete inverse theory. Academic Press inc.

RMT-F, 2005. RMT-F1 and SM25 user manual. Microkor and St. Petersburg University.

Scholl, C., 2005. The influence of multidimensional structures on the interpretation of LOTEM data with one-dimensional models and the application to data from Israel. Ph.D. thesis, Universität zu Köln, Institut für Geophysik und Meteorologie.

SFB-806, January 2012. OUR WAY TO EUROPE-Culture-Environment Interaction and Human Mobility in the Late Quaternary. Online.
URL http://www.sfb806.uni-koeln.de/

Spies, B. R., Frischknecht, F. C., 1991. Electromagnetic Sounding. In: Nabighian, M. N. (Ed.), Electromagnetic methods in applied geophysics. Vol. 2. Soc. Expl. Geophys., Ch. 5.

Tezkan, B., 2009. Radiomagnetotellurics, in Groundwater Geophysics, A Tool for Hydrogeology, 2nd Edition. Springer-Verlag, Ed. by R. Kirsch, Ch. 10, pp. 295–316.

Tezkan, B., Saraev, A., 2007. On the 2D inversion of radiomagnetotelluric data (10 kHz-1 MHz) for shallow investigations observed by a newly developed device. Near Suface Geophysics 6, 245–252.

Ward, S. H., Hohmann, G. W., 1988. Electromagnetic theory for geophysical applications. Soc. Explor. Geophys., eM, theory.

Zonge, Mai 2002. GDP-32 II Multifunction Receiver Operation Manual. Zonge Engineering and Research Organization.
URL http://www.zonge.com/RxManuals.html